

Aerial Height Prediction and Refinement Neural Networks with Semantic and Geometric Guidance

Mahdi Elhousni, Ziming Zhang and Xinming Huang

Abstract—Deep learning provides a powerful new approach to many computer vision tasks. Height prediction from aerial images is one of those tasks that benefited greatly from the deployment of deep learning which replaced traditional multi-view geometry techniques. This manuscript proposes a two-stage approach, where the first stage is a multi-task neural network whose main branch is used to predict the height map resulting from a single RGB aerial input image, while being augmented with semantic and geometric information from two additional branches. The second stage is a refinement step, where a denoising autoencoder is used to capture the imperfections in the first prediction, in order to produce a more accurate height map. Experiments on two publicly available datasets show that the proposed method is able to outperform state-of-the-art deep learning based height prediction networks. Code is publicly available¹.

Index Terms—UAV, Height, DSM, CNN, Autoencoders, Multi-Task.

I. INTRODUCTION

THE analysis of aerial imagery was well-known to be a very tedious task due to the low quality of the acquired images and the lack of some appropriate automated process that could extract the relevant information from the data. This of course changed, when advances were made in computer vision that made it possible extract predefined patterns, by using carefully designed algorithms. However, with the recent development of deep learning, the democratization of personal quad-copters, in addition to the increased investment in quality satellite imagery, brought a new revolution to the field of aerial imagery analysis. As a result of that, multiple deep learning challenges related to aerial imagery processing such as : semantic segmentation [1], [2] or object detection [3], [4], have been routinely featured in numerous challenges offered each year by the GRSS community [5]–[7].

We focus on the height prediction task, where based on an input RGB aerial image, we are supposed to predict and reconstruct the corresponding height map, or in other words, predict the height value of each pixel in the input image. Predicting such height maps can be very useful in subsequent UAV related challenges such as building and roof reconstruction or 3D mesh production. By obtaining the accurate height of each building or structure appearing in the input images, 3D models generated by any method could be refined by using our height prediction pipeline, in order to produce accurate representations of the surrounding world. These 3D models

The authors are with the Electrical and Computer Engineering Department, at the Worcester Polytechnic Institute, 100 Institute Rd, Worcester, MA 01609 (emails: {melhousni, zzhang15, xhuang}@wpi.edu)

¹https:

github.com/melhousni/DSMNet

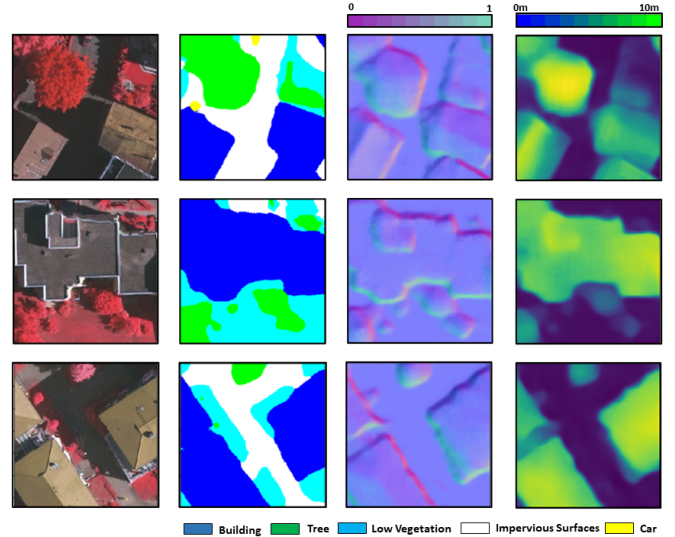


Fig. 1. The outputs of our multi-task network. From left to right: The input RGB image, the output semantic labels, surface normals and height predictions.

can be crucial for real-world applications such as accurate UAV navigation or urban planning. These reconstructions are traditionally done using Structure from Motion (SfM) [8], [9] and stereo camera rigs, which can be very sensible to noise and changes in lightning conditions. On the other hand, more methods revolving around deep learning networks have been presented in the literature lately and show great potential.

We explore this challenge through a multi-task learning framework where additional results are produced and used to improve the main height prediction results. Previous works have already proposed and showed that multi-task learning helps improving the accuracy of height prediction networks by including semantic labels. We propose to add a third branch in our multi-task network which will be devoted to predicting the surface normals, as shown on Fig. 1. In this configuration, the main height prediction branch will have access to both semantic and geometric guidance, helping it to predict height values more accurately. Those outputs can themselves be combined with the height prediction in a later step to produce semantic 3D models or higher quality 3D meshes.

However, since our only input is a single RGB image, our predictions are bound to be noisy due to artefacts such as shadows or unexpected changes in color. Therefore, we also propose to introduce a refinement step where the output from

the first stage prediction is fed to a denoising auto-encoder in order to remove the noise and produce higher quality and more accurate height maps. By combining these two steps, we are able to produce results that surpass the current state-of-the-art on multiple datasets. We are also able to produce reasonable semantic labels and surface normals prediction without explicitly optimizing those results.

Specifically, our contributions in this work are the following:

- We propose a triple-branch network, based on pretrained off-the-shelf encoders, for semantic labels, surface normals and height prediction.
- We introduce a denoising autoencoder as a refinement step for our final height maps.
- We achieve state-of-the-art performance on two publicly available datasets, and an extensive ablation study shows the importance of each step in our reconstruction pipeline.
- We demonstrate through two applications how our height prediction pipeline can be used to reconstruct dense 3D pointclouds, which themselves can be extended to semantic pointclouds and 3D meshes.

II. RELATED WORK

Multi-task learning: This learning framework aims at optimizing (through back propagation in this case) a single neural network with the goal of predicting multiple related outputs, represented by multiple task-specific loss functions [10]. Lately, this approach has become increasingly more popular, especially in the area of autonomous driving cars [11], [12], where multiple results (such as moving objects, driveable areas, agents behaviour) are derived simultaneously from the input camera data.

Height prediction from aerial images: This task has been receiving increasing attention by the deep learning and remote sensing communities, especially after the use of UAVs to collect aerial data has become widespread and accessible. The goal here is to generate height value for each pixel in an input aerial image. In works such as [13]–[15], deep learning methods and techniques such as residual networks, skip connections and generative adversarial networks are leveraged in order to predict the expected height maps.

Other works such as [16], [17], proposed to reformulate the task as a multi-learning problem, by introducing neural networks capable of predicting both the height maps and the semantic labels simultaneously. These works showed that both outputs benefit from the presence of the other, during the simultaneous optimization process of the multi-task network. We chose to extend that formulation by including a third branch in our network, tasked with predicting surface normals, which was inspired by previous works [18], [19] in the depth prediction task for autonomous driving cars. Surface normals are also known to be extremely useful during 3D reconstruction tasks and is required for surface and mesh reconstruction algorithms such as the Poisson surface reconstruction algorithm [20] or the Ball pivoting algorithm [21].

Denoising Autoencoders: Removing noise from images is a challenge as old as computer vision itself. Over the years, multiple techniques were proposed in the literature which can

be broadly divided into two categories [22] : spatial filtering methods, and variational denoising methods. The spatial filtering methods can either be linear, such as Mean filtering [23] or Wiener filtering [24], [25], or non linear such as median filtering [26] or bilateral filtering [27]. These filtering methods work reasonably to a certain extent. However, when the noise level is too high, these methods tend to lead to an over-smoothing of the input images and the edges present in them. On the other hand, in variational denoising methods, an energy function is defined and minimized to remove the noise, based on image priors and noise free images. Some popular variational denoising methods are: Total variation regularization [28], Non-local regularization [29] and Low-rank minimization [30].

Lately however, a new trend based on deep learning autoencoders has shown great potential : Autoencoders are a popular neural network architecture that has shown to be powerful across multiple tasks such as segmentation of medical imagery [31], decoding the semantic meaning of words [32] or solving facial recognition challenges [33]. One of the most useful type of autoencoders available in the literature is the denoising autoencoder: [34] has shown that autoencoders can be trained and used to remove noise from an arbitrary input signal such as an image. We propose to use denoising autoencoder to refine the height prediction of our multi-task learning network.

III. METHOD

A. Problem setup

Our main objective here is to predict an accurate height map using only a monocular aerial image as input. Fundamentally, we are trying to solve a non-linear regression problem which can be formulated as:

$$\min_{\psi \in \Psi} \sum_i \ell(\mathbf{y}_i, \psi(\mathbf{x}_i)) \quad (1)$$

where $\psi : \mathcal{X} \rightarrow \mathcal{Y}$ denotes the height prediction mapping function from the feasible space Ψ , $\ell : \mathcal{Y} \times \mathcal{Y} \rightarrow \mathbb{R}$ denotes a loss function such as the least-square, \mathbf{x}_i is the input aerial image and y_i is the output height map.

Predicting height only using a single aerial image is possible. However, previous works such as [16], [17] showed that including additional branches to predict other related information such as segmentation labels can be beneficial for both tasks. In our case, in addition to predicting the height maps, we also predict semantic labels and surface normals, which provide semantic and geometric guidance by augmenting the main height branch with information from the semantics and normals branches. More details on this can be found in the height prediction section below. Keeping that in mind, our ψ function can now be defined as:

$$\psi(\mathbf{x}_i) = \{\mathbf{P}_h, \mathbf{P}_s, \mathbf{P}_n\} \quad (2)$$

where \mathbf{P}_h , \mathbf{P}_s and \mathbf{P}_n are the height, semantic and surface normal predictions respectively, that are trying to approximate $\mathbf{y}_i = \{\mathbf{P}_h^*, \mathbf{P}_s^*, \mathbf{P}_n^*\}$ where \mathbf{P}_h^* , \mathbf{P}_s^* and \mathbf{P}_n^* are the height,

semantic and surface normal ground truth respectively. Finding a good approximation of the ψ function can be seen as the first stage in our proposed method.

Regression problems such as the one we are facing are difficult to solve due to the high number of values expected to be predicted. This makes our height prediction \mathbf{P}_h noisy by definition, so the use of denoising autoencoders is appropriate in this situation.

First, we can write: $\mathbf{P}_h = \mathbf{P}'_h + e$ where \mathbf{P}'_h is the clean height value, and e the noise inherent to our approximation of the function ψ . By introducing a denoising autoencoder, we can approximate the noise function γ such as $\mathbf{P}_h = \mathbf{P}'_h + \gamma(\mathbf{z}_i)$, where \mathbf{z}_i is the concatenation of the outputs of ψ with the input aerial image x_i . This makes it possible to re-write equations (2) as $\psi(\mathbf{x}_i) = \{\mathbf{P}'_h + \gamma(\mathbf{z}_i), \mathbf{P}_s, \mathbf{P}_n\}$. We can also now define the objective of the second stage of our method such as:

$$\min_{\gamma \in \Gamma} \sum_i \ell(\mathbf{P}_h^*, \mathbf{P}_h - \gamma(\mathbf{z}_i)) \quad (3)$$

In this paper, our goal is to approximate both function ψ and γ by using two cascaded deep neural networks.

B. Height prediction

We solve the height prediction problem here via multi-task learning where, in addition to the main height prediction, semantic and surface normals predictions are conducted too. We found that by re-routing the information in the semantic and surface normal branches to the main height branch, our neural network can learn to predict better values, especially around edges.

We solve the height prediction problem here via multi-task learning where, in addition to the main height prediction, semantic and surface normals predictions are conducted too. We found that by re-routing the information in the semantic and surface normal branches to the main height branch, our neural network can learn to predict better values, especially around edges.

Fig. 2 shows our multi-task learning network architecture. We propose a neural network where we combine a pre-trained encoder (tasked with extracting relevant features from the input aerial images), with three inter-connected decoder branches for each of the three expected predictions. We choose to use a DenseNet121 network, pretrained on ImageNet, as our main encoder. We show later in the experimentation part that compared to other popular architectures, DenseNet121 yields the best accuracy. Our decoders on the other hand is inspired by [35] and are characterized by being able to reconstruct the expected predictions efficiently. We list in Table I the different layers that we used.

This network is optimized by using a multi-objective loss function defined as:

$$\mathcal{L} = w_1 \mathcal{L}_h + w_2 \mathcal{L}_s + w_3 \mathcal{L}_n \quad (4)$$

where $\mathcal{L}_h = \frac{1}{n} \sum_{i=1}^n (P_h - P_h^*)^2$, $\mathcal{L}_s = -\frac{1}{n} \sum_{i=1}^n P_s^* \log(P_s)$, $\mathcal{L}_n = \frac{1}{n} \sum_{i=1}^n (P_n - P_n^*)^2$ and

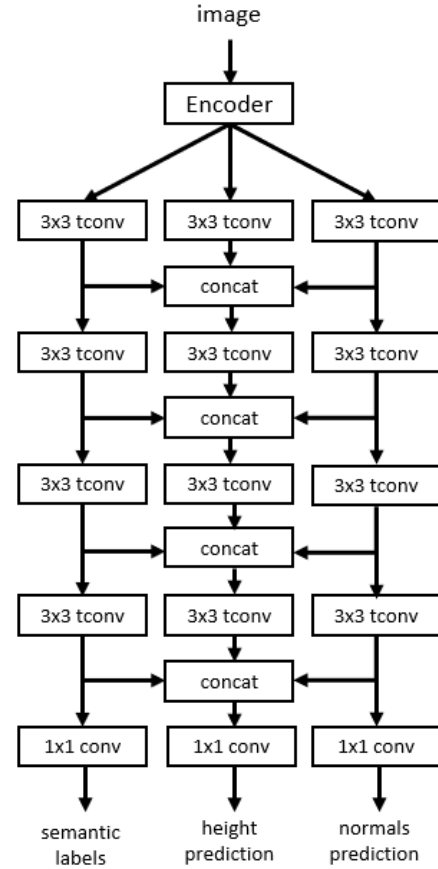


Fig. 2. Architecture of our multi-task learning network for height, semantic and surface normals predictions. Note that each tconv block is followed by the ReLU function and drop out layers are inserted after each tconv layers in the main height prediction branch.

w_1 , w_2 and w_3 are weights set up according to the training dataset and the scale of each loss function.

C. Height refinement

As mentioned before, our height prediction map \mathbf{P}_h is noisy and can be considered an initial guess at the final height prediction \mathbf{P}'_h . We introduce an autoencoder in order to estimate the noise and produce more accurate height map predictions.

We choose the popular U-Net architecture [31] as network structure, and use as an input the concatenation of the outputs from the previous multi-task network $\mathbf{P}_h, \mathbf{P}_s$ and \mathbf{P}_n with the aerial image \mathbf{x}_i , as shown in Fig. 3. Details of the different layers forming the denoising network are listed in Table II. The loss function used to optimize this network is the mean square error between the refined height map and the ground truth: $\mathcal{L}_r = \frac{1}{n} \sum_{i=1}^n (P'_h - P_h^*)^2 = \frac{1}{n} \sum_{i=1}^n (P_h - \gamma - P_h^*)^2$, with γ being the noise function defined in Eq. 3.

IV. EXPERIMENTS

A. Datasets

2018 DFC [36]: This dataset was released during the 2018 Data Fusion Contest organized by the Image Analysis and

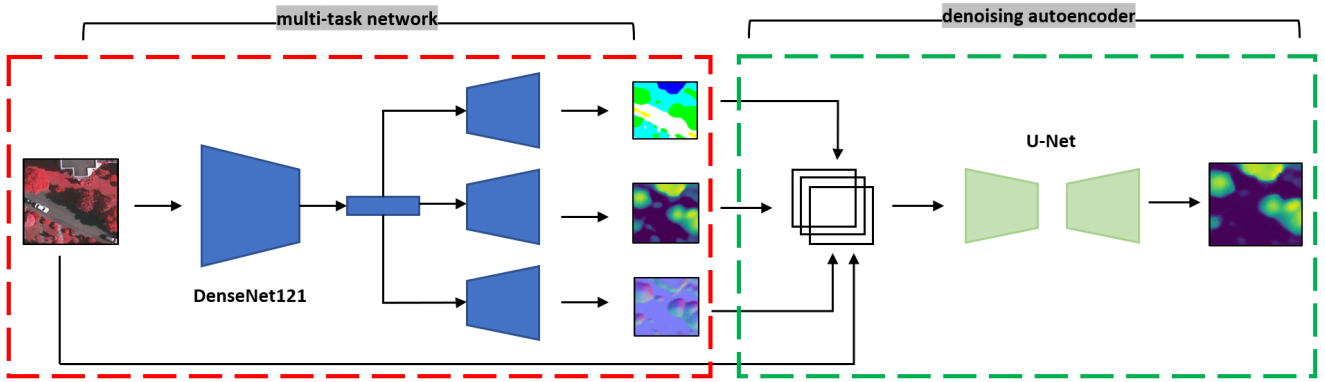


Fig. 3. Our two stage height prediction and refinement pipeline. We use DenseNet121 to extract a global feature vector from the input aerial images, which is used to predict the normals map, semantic labels and a first guess at the height map (first stage, in red). These results are concatenated with the input aerial image and fed into a denoising autoencoder to generate the refined final height map (second stage, in green).

TABLE I
HEIGHT PREDICTION NETWORK DETAILS.

	Layer	Output Size
Encoder	DenseNet121	(10,10,1024)
Decoder	<i>DeConv</i> ₁	(20,20,1024)
	<i>Concat</i>	(20,20,3072)
	<i>Conv</i> ₁₁	(20,20,1024)
	<i>Conv</i> ₁₂	(20,20,1024)
	<i>DeConv</i> ₂	(40,40,512)
	<i>Concat</i>	(40,40,1536)
	<i>Conv</i> ₂₁	(40,40,512)
	<i>Conv</i> ₂₂	(40,40,512)
	<i>DeConv</i> ₃	(80,80,256)
	<i>Concat</i>	(80,80,768)
	<i>Conv</i> ₃₁	(80,80,256)
	<i>Conv</i> ₃₂	(80,80,256)
	<i>DeConv</i> ₄	(160,160,64)
	<i>Concat</i>	(160,160,192)
	<i>Conv</i> ₄₁	(160,160,64)
	<i>Conv</i> ₄₂	(160,160,64)
	<i>DeConv</i> ₅	(320,320,32)
<i>Concat</i>	(320,320,96)	
<i>Conv</i> ₅₁	(320,320,32)	
<i>Conv</i> ₅₂	(320,320,32)	
	<i>Conv</i> _{out}	(320,320,1)

TABLE II
HEIGHT REFINEMENT NETWORK DETAILS.

	Layer	Output Size
Encoder	<i>Conv</i> ₁	(320,320,64)
	<i>MaxPooling</i>	(160,160,64)
	<i>Conv</i> ₂	(160,160,128)
	<i>MaxPooling</i>	(80,80,128)
	<i>Conv</i> ₃	(80,80,256)
	<i>MaxPooling</i>	(40,40,256)
	<i>Conv</i> ₄	(40,40,512)
Decoder	<i>MaxPooling</i>	(20,20,512)
	<i>Conv</i> ₅	(20,20,1024)
	<i>Upsampling</i>	(40,40,512)
	<i>Concat</i>	(40,40,1024)
	<i>Conv</i> ₆	(40,40,512)
	<i>Upsampling</i>	(80,80,256)
	<i>Concat</i>	(80,80,512)
	<i>Conv</i> ₇	(80,80,256)
	<i>Upsampling</i>	(160,160,128)
	<i>Concat</i>	(160,160,256)
<i>Conv</i> ₈	(160,160,128)	
<i>Upsampling</i>	(320,320,64)	
<i>Concat</i>	(320,320,128)	
<i>Conv</i> ₈	(320,320,64)	
	<i>Conv</i> _{out}	(320,320,1)

Data Fusion Technical Committee of the IEEE Geoscience and Remote Sensing Society. It was collected over the city of Houston, and contains multiple optical resources geared toward urban machine learning tasks such as multispectral LiDAR, hyperspectral imaging, Very High-Resolution (VHR) imagery and semantic labels. Using the results of the multispectral LiDAR, it is possible to generate Digital Structural Models (DSM) and Digital Elevation Models (DEM), which, if subtracted from one another, produces height maps that we can use as ground truth. 4 tiles are used for training while 10 are used for testing.

ISPRS Vaihingen [37] : This dataset was released during the semantic labeling contest of ISPRS WG III/4. It was collected over the city of Vaihingen, Germany and consists of very high resolution true ortho photo (TOP) tiles and corresponding Digital Surface Models (DSM) and semantic labels. As it is usually done when dealing with this dataset, we use the normalized DSM (nDSM) produced by [38] as

ground truth for our height prediction. 16 tiles were used for training while 17 tiles are used for testing.

Surface normal maps : The surface normal maps for both dataset are generated using the given height maps, following practices usually used for surface normals estimation from dense depth maps based on the Sobel operator [39]. The details are listed in Alg 1.

Algorithm 1: Surface normals generation

Input : Height map P_h

Output: Surface normals map P_n

$zx \leftarrow Sobel(P_h, 0)$

$zy \leftarrow Sobel(P_h, 1)$

$N \leftarrow stack(-zx, -zy, 1)$

$P_n \leftarrow \frac{N/\|N\|}{2} + 1$

return P_n

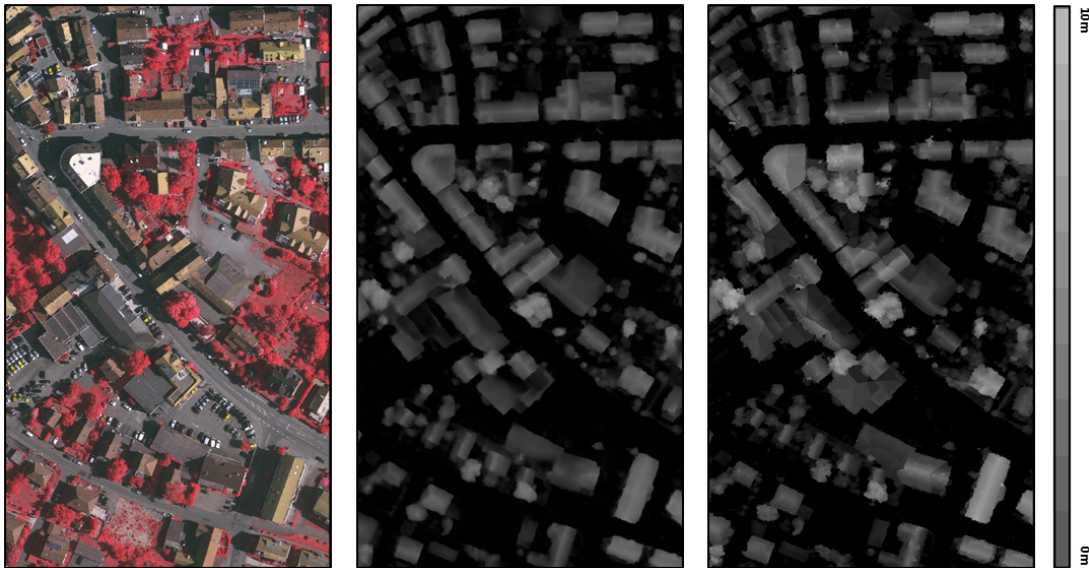


Fig. 4. Qualitative comparison of a reconstructed tile from the testing dataset. From left to right: The input RGB tile, the height prediction and the height ground truth.

B. Height prediction and refinement

Training : Our training process is not end-to-end. Instead, we follow a two stages approach: we first remove the denoising autoencoder and only focus on training the multi-task network. To do so, random 320x320 crops are sampled from the aerial tiles and corresponding semantic, surface normals and height ground truth, and are used for training. Once the multi-task network converges, we freeze its weights and plug in the denoising autoencoder to refine our height predictions. We train this second network following the same random sampling process used to train the first one. We use Tensorflow [40], a learning rate of 0.0002, the Adam optimizer [41] and a single RTX2080Ti to train both stages.

Note that in the case of the DFC2018 dataset, the input VHR aerial tiles are ten times bigger than their corresponding DSM, DEM and semantic labels. To deal with that, we first down sample the aerial tiles ten times before starting to collect training crops.

Results : The aerial tiles were reconstructed using a rolling window of the same size of the training samples and with a constant step size. We use Gaussian smoothing to deal with overlapping areas. We report the results of our height prediction and refinement pipeline on both the datasets cited before in Table III in meters and show a qualitative comparison in Fig. 4. When comparing with previous proposed methods in the literature, we can see that by using our multi task network combined with our refinement step, we are able to surpass the state-of-the-art scores across all metrics on both datasets, with sometimes improvement up to 25%.

It is especially interesting to note that we are able to achieve similar scores to methods which were trained on the VHR aerial tiles directly without any down sampling as shown in Table IV. Such networks would need much longer time than our method to reconstruct the same size output height tiles.

Missing values in Table III were not reported by the cited publications. We also exclude the results reported by [15] because they do not follow the official training/testing split of the data.

TABLE III
COMPARISON WITH OTHER HEIGHT PREDICTION METHODS ON THE ISPRS VAIHINGEN AND THE 2018 DFC DATASETS IN METERS.

Method	ISPRS Vaihingen			2018 DFC		
	MSE	MAE	RMSE	MSE	MAE	RMSE
Ours	0.0042	0.036	0.062	6.92	1.37	2.57
Carvalho [16]	0.0060	0.045	0.074	9.34	1.53	2.97
Srivastava [17]	-	0.063	0.098	-	-	-
IMG2DSM [14]	-	-	0.090	-	-	-

TABLE IV
COMPARISON WITH METHOD TRAINED ON VHR AERIAL IMAGES.

Method	MSE	MAE	RMSE	Time (s)	Input Resolution
Ours	6.92	1.37	2.57	72	1192x1202
Carvalho VHR [16]	7.27	1.26	2.59	774	11920x12020

C. Semantic label and surface normal predictions

Even though we do not focus on the semantic label and surface normal predictions and only use them to improve the height predictions, we share the results of those two branches and compare them with available methods in the literature in Table V. Our results in Table V and Fig. 5 show that our multi-task network is able to produce semantic label results that are comparable with the state of the art on the Vaihingen dataset and acceptable ones on the DFC2018 (which has 20 classes compared to the 6 of the Vaihingen dataset). It is also able to produce meaningful surface normal maps as seen on Fig. 6. Missing values in Table V were not reported by the cited publications.

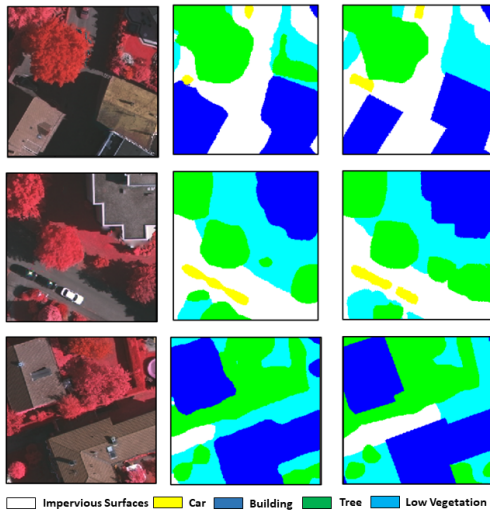


Fig. 5. Qualitative comparison. From left to right: The input RGB image, the semantic prediction, the semantic ground truth.

TABLE V

SEMANTIC LABELS AND SURFACE NORMALS RESULTS ON THE ISPRS VAIHINGEN AND THE 2018 DFC DATASETS.

Method	ISPRS Vaihingen			2018 DFC		
	OA	AA	Kappa	OA	AA	Kappa
Ours	85.6	74.8	80.1	51.89	47.01	49
Carvalho [16]	87.7	85.4	75.9	64.70	58.85	63
Srivastava [17]	78.8	73.4	71.9	-	-	-
Cerra [42]	-	-	-	58.60	55.60	56
Fusion-FCN [43]	-	-	-	63.28	-	61
Surface Normals						
Method	MSE	MAE	RMSE	MSE	MAE	RMSE
Ours	0.0115	0.0642	0.1066	0.0620	0.2119	0.2572

D. Ablation study

Height refinement : To demonstrate the usefulness of our additional refinement step. we test our method with and without the denoising autoencoder, on both available datasets. In Table VI, we compare the results obtained after both experiments and show that the refinement step always produces more accurate height maps, bringing sometimes an increase of up to 16% in accuracy. Additionally, we compare our deep learning based denoiser with other popular non-learning denoising algorithms such as Bilateral Filtering (BF) [27] and Non-local Means (NIM) regularization [29].

TABLE VI

COMPARISON OF OUR HEIGHT PREDICTION METHODS WITH AND WITHOUT REFINEMENT, ON THE ISPRS VAIHINGEN AND THE 2018 DFC DATASETS IN METERS.

Method	ISPRS Vaihingen			2018 DFC		
	MSE	MAE	RMSE	MSE	MAE	RMSE
multi-task only	0.0045	0.043	0.065	7.36	1.50	2.64
multi-task + BF	0.0046	0.043	0.065	7.27	1.51	2.62
multi-task + NIM	0.0045	0.043	0.065	7.34	1.48	2.63
multi-task + Unet	0.0042	0.036	0.062	6.92	1.37	2.57

We also show qualitatively on Fig. 7 that the refinement height maps are much closer to the ground truth and contains

less noise than the direct output of the multi-task network.

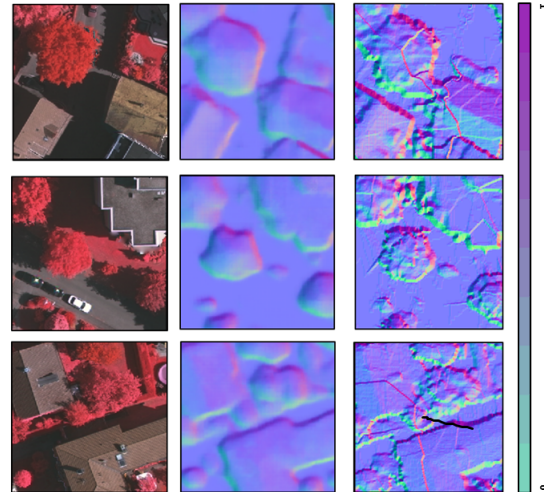


Fig. 6. Qualitative comparison. From left to right: The input RGB image, the surface normals prediction, the surface normals ground truth.

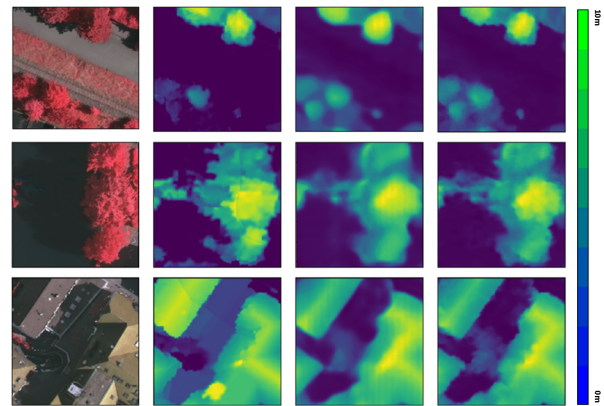


Fig. 7. Qualitative comparison. From left to right: The input RGB image, the height prediction of our multi-task network, the refined height map of our denoising autoencoder and the ground truth.

Choosing the right encoder : Our network structure for height prediction is flexible, since any off-the shelf encoder can be used in the first stage to extract features from the input aerial image.

TABLE VII

ENCODER COMPARISON ON THE DFC2018 DATASET IN METERS.

Encoder	MSE	MAE	RMSE
ResNet101 [44]	18.95	3.33	4.19
VGG19 [45]	8.57	1.87	2.85
DenseNet121 [46]	7.36	1.50	2.64

However, we show in Table VII that DenseNet121 outperforms other popular encoder structures and produces the most accurate height maps. To ensure fairness, all the networks were trained for the same number of epochs and using the same hyper parameters, in order for us to be able to compare both the convergence speed and accuracy scores.

Geometric and semantic guidance : We show in this section, the effect of the geometric and semantic guidance on our method in both the prediction and refinement stages. First, we show in Table VIII that using a multi-task network instead of a single-task one, with three branches for height, semantic labels and surface normals, improves our overall height prediction results. We also show in Table IX that by concatenating all the results of the first stage as the input to the denoising autoencoder, we are able to generate more accurate and refined results compared to only using the height image as input.

TABLE VIII
COMPARISON OF HEIGHT PREDICTION RESULTS OF SINGLE AND MULTI-TASK NETWORKS IN METERS.

Method	ISPRS Vaihingen			2018 DFC		
	MSE	MAE	RMSE	MSE	MAE	RMSE
single-task	0.0048	0.046	0.067	8.17	1.64	2.78
multi-task	0.0045	0.043	0.065	7.36	1.50	2.64

TABLE IX
COMPARISON OF HEIGHT REFINEMENT RESULTS OF SINGLE AND MULTI-INPUT DENOISER IN METERS.

Method	ISPRS Vaihingen			2018 DFC		
	MSE	MAE	RMSE	MSE	MAE	RMSE
single-input	0.0043	0.037	0.063	7.13	1.47	2.62
multi-input	0.0042	0.036	0.062	6.92	1.37	2.57

Finding the right reconstruction step : The accuracy of our final tile reconstruction depends also on the step size of the rolling window that we use when collecting aerial crops. We show in Table X the different results corresponding to different step sizes. We found that a step size of 60 is the most optimal one across both datasets.

TABLE X
COMPARISON OF OUR RECONSTRUCTION RESULTS (METERS) BASED ON THE STEP SIZE (PIXELS).

Step	ISPRS Vaihingen			2018 DFC		
	MSE	MAE	RMSE	MSE	MAE	RMSE
80	0.00421	0.0363	0.0625	6.98	1.38	2.58
60	0.00420	0.0362	0.0623	6.92	1.37	2.57
40	0.00421	0.0362	0.0623	6.93	1.37	2.58

Visualizing the uncertainty : In order to investigate the performance of our pipeline more thoroughly, we generate uncertainty maps according to the method proposed in [47]. The results are displayed in Fig. 8 and show that most of the prediction errors can be attributed to the areas such as the edges of buildings due to the sudden changes in brightness and color, and trees where shadows introduce a significant amount of color noise.

V. APPLICATIONS

In this section, we propose two applications to show how to take advantage of the results generated by our proposed pipeline: One application is 3D reconstruction of select buildings from a single aerial image. In the other application, we

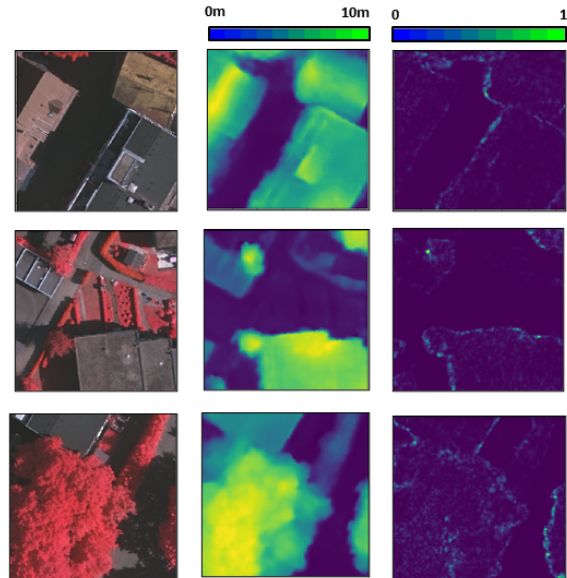


Fig. 8. Uncertainty results. From left to right RGB Image, Height Prediction, Uncertainty Map. Prediction errors are mostly concentrated around the edges.

simulate a UAV flight over a certain area and show that we can reconstruct the entire area by combining odometry and aerial images. In comparison to the classic SfM algorithm, our method provides a significant gain in speed, accuracy and density. More importantly, our proposed method requires significantly less number of images since only minimal overlaps are necessary when taking the aerial shots.

A. Single aerial image 3D reconstruction

Usually, in order to reconstruct the 3D shape of a building, multiple shots from multiple angles with significant overlap are necessary in order to apply the sequential surface from motion algorithm. We show in Fig. 9(b) that owing to our multi-task network, we are able to produce accurate 3D pointclouds of the buildings using a single image only.

We also show that we are capable of generating semantic pointclouds in Fig. 9(c) and 3D meshes of buildings and their surrounding areas in Fig. 9(d) by leveraging the semantic labels and surface normals generated by our networks. Specifically, semantic pointclouds are generated by projecting the semantic labels onto the pointclouds, while the meshes are generated by combining the outputted surface normals and the reconstructed pointclouds with the ball pivoting algorithm [21].

B. Area reconstruction with simulated UAV flight

3D reconstruction of urban areas is a very important task. Similarly to what we mentioned in our first application, reconstructing an entire area would generally require a series of captured images with significant overlap, and potentially multiple passes of the same area, in order to generate a semi-dense pointcloud.

In our case, we show in Fig. 10 that by using a single pass, with a small number of captured images and minimal overlap

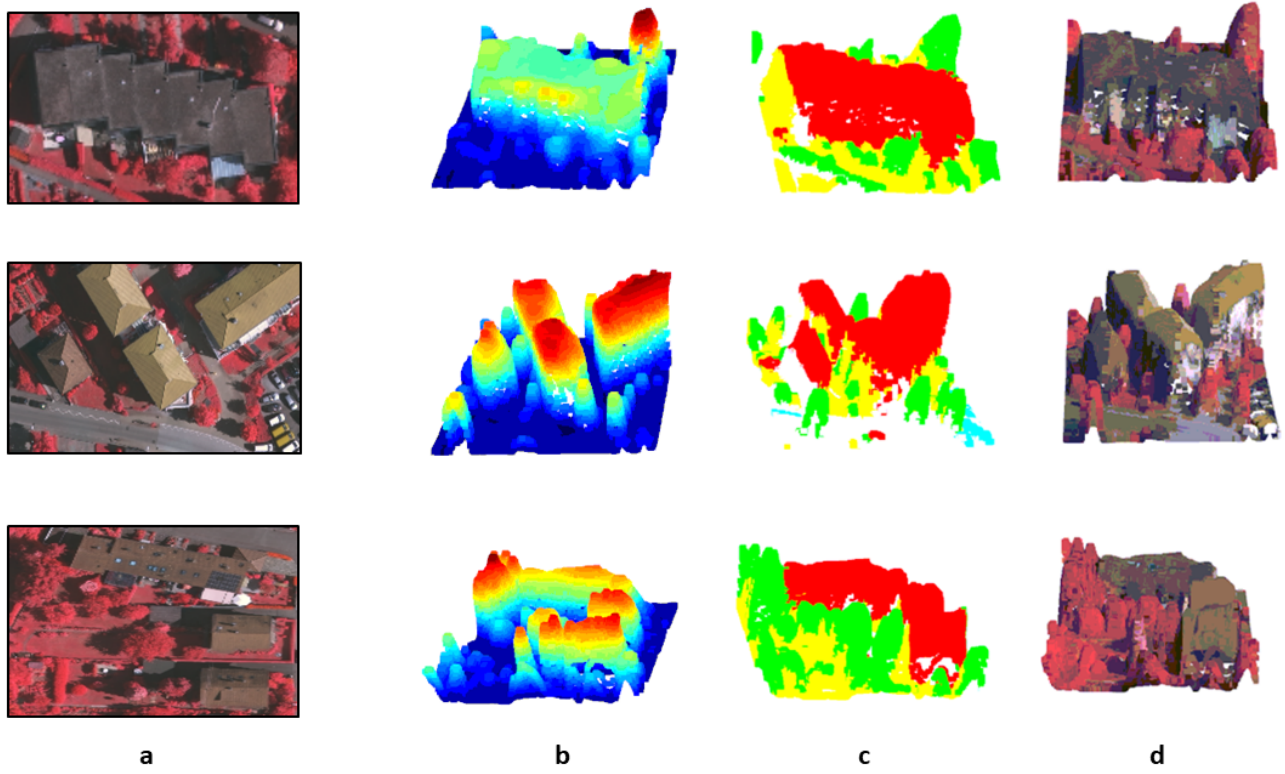


Fig. 9. 3D reconstructions using a single image. (a) RGB Image, (b) Height Colorized Pointcloud, (c) Semantic Pointcloud, (d) RGB Colorized Mesh.

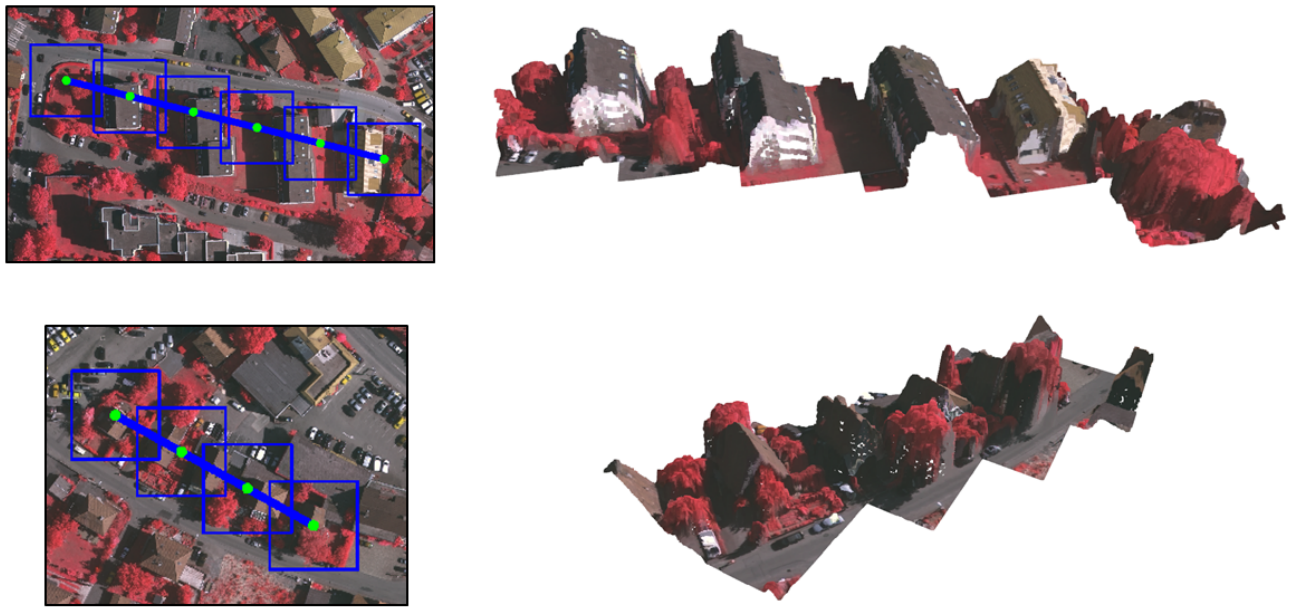


Fig. 10. 3D reconstructions from simulated UAV flight. From left to right : Positions of the UAV images, Reconstructed 3D scene.

(only to avoid gaps in the final reconstruction) we are able to produce accurate and dense 3D reconstructions. We also note that when we feed the same data to a SfM algorithm, it typically leads to failure due to the small number of features that can be matched among the single-pass shots. The data is collected by simulating a constant altitude UAV flight over a certain neighborhood in one of the tiles available in the testing datasets. The odometry is assumed to be known from an onboard IMU or GPS sensors.

VI. CONCLUSION

In this work, we propose a two-stage pipeline to predict and refine height maps using only an RGB aerial image as input. We leverage the power of multi-task learning by designing a three-branch neural network for height, semantic labels and surface normals prediction. We also introduce a denoising autoencoder to refine the predicted height maps and eliminate the noise inherent to the output of our first stage network and the ambiguities sometimes present in RGB images. Experiments on two publicly available datasets show that our method is capable of outperforming state-of-the-art results in height prediction. In future work, we plan on exploring the computational efficiency of the proposed neural networks and their applications in real-time processing of UAV aerial images.

REFERENCES

- [1] K. Chen, K. Fu, M. Yan, X. Gao, X. Sun, and X. Wei, "Semantic segmentation of aerial images with shuffling convolutional neural networks," *IEEE Geoscience and Remote Sensing Letters*, vol. 15, no. 2, pp. 173–177, 2018.
- [2] D. Marmanis, J. D. Wegner, S. Galliani, K. Schindler, M. Datcu, and U. Stilla, "Semantic segmentation of aerial images with an ensemble of cnns," *ISPRS Annals of the Photogrammetry, Remote Sensing and Spatial Information Sciences*, 2016, vol. 3, pp. 473–480, 2016.
- [3] J. Ding, N. Xue, Y. Long, G.-S. Xia, and Q. Lu, "Learning roi transformer for oriented object detection in aerial images," in *Proceedings of the IEEE Conference on Computer Vision and Pattern Recognition*, 2019, pp. 2849–2858.
- [4] I. Ševo and A. Avramović, "Convolutional neural network based automatic object detection on aerial images," *IEEE geoscience and remote sensing letters*, vol. 13, no. 5, pp. 740–744, 2016.
- [5] B. Le Saux, N. Yokoya, R. Hansch, and S. Prasad, "2018 ieec grss data fusion contest: Multimodal land use classification [technical committees]," *IEEE geoscience and remote sensing magazine*, vol. 6, no. 1, pp. 52–54, 2018.
- [6] B. Le Saux, N. Yokoya, R. Hansch, M. Brown, and G. Hager, "2019 data fusion contest [technical committees]," *IEEE Geoscience and Remote Sensing Magazine*, vol. 7, no. 1, pp. 103–105, 2019.
- [7] N. Yokoya, P. Ghamisi, R. Hänsch, and M. Schmitt, "2020 ieec grss data fusion contest: Global land cover mapping with weak supervision [technical committees]," *IEEE Geoscience and Remote Sensing Magazine (GRSM)*, vol. 8, no. 1, pp. 154–157, 2020.
- [8] P. Moulon, P. Monasse, and R. Marlet, "Adaptive structure from motion with a contrario model estimation," in *Asian Conference on Computer Vision*. Springer, 2012, pp. 257–270.
- [9] P. Moulon and P. Monasse, "Global fusion of relative motions for robust, accurate and scalable structure from motion," in *Proceedings of the IEEE International Conference on Computer Vision*, 2013, pp. 3248–3255.
- [10] R. Caruana, "Multitask learning," *Machine learning*, vol. 28, no. 1, pp. 41–75, 1997.
- [11] M. Teichmann, M. Weber, M. Zoellner, R. Cipolla, and R. Urtasun, "Multinet: Real-time joint semantic reasoning for autonomous driving," in *2018 IEEE Intelligent Vehicles Symposium (IV)*. IEEE, 2018, pp. 1013–1020.
- [12] D. Zhou, J. Fang, X. Song, L. Liu, J. Yin, Y. Dai, H. Li, and R. Yang, "Joint 3d instance segmentation and object detection for autonomous driving," in *Proceedings of the IEEE/CVF Conference on Computer Vision and Pattern Recognition (CVPR)*, June 2020.
- [13] H. A. Amirkolaei and H. Arefi, "Height estimation from single aerial images using a deep convolutional encoder-decoder network," *ISPRS journal of photogrammetry and remote sensing*, vol. 149, pp. 50–66, 2019.
- [14] P. Ghamisi and N. Yokoya, "Img2dsm: Height simulation from single imagery using conditional generative adversarial net," vol. 15, no. 5. IEEE, 2018, pp. 794–798.
- [15] C.-J. Liu, V. A. Krylov, P. Kane, G. Kavanagh, and R. Dahyot, "Im2elevation: Building height estimation from single-view aerial imagery," *Remote Sensing*, vol. 12, no. 17, p. 2719, 2020.
- [16] M. Carvalho, B. Le Saux, P. Trouvé-Peloux, F. Champagnat, and A. Almansa, "Multitask learning of height and semantics from aerial images." *IEEE Geoscience and Remote Sensing Letters*, 2019.
- [17] S. Srivastava, M. Volpi, and D. Tuia, "Joint height estimation and semantic labeling of monocular aerial images with cnns," in *2017 IEEE International Geoscience and Remote Sensing Symposium (IGARSS)*. IEEE, 2017, pp. 5173–5176.
- [18] T. Dharmasiri, A. Spek, and T. Drummond, "Joint prediction of depths, normals and surface curvature from rgb images using cnns," in *2017 IEEE/RSJ International Conference on Intelligent Robots and Systems (IROS)*. IEEE, 2017, pp. 1505–1512.
- [19] D. Eigen and R. Fergus, "Predicting depth, surface normals and semantic labels with a common multi-scale convolutional architecture," in *Proceedings of the IEEE international conference on computer vision*, 2015, pp. 2650–2658.
- [20] M. Kazhdan, M. Bolitho, and H. Hoppe, "Poisson surface reconstruction."
- [21] F. Bernardini, J. Mittleman, H. Rushmeier, C. Silva, and G. Taubin, "The ball-pivoting algorithm for surface reconstruction," *IEEE transactions on visualization and computer graphics*, vol. 5, no. 4, pp. 349–359, 1999.
- [22] L. Fan, F. Zhang, H. Fan, and C. Zhang, "Brief review of image denoising techniques," *Visual Computing for Industry, Biomedicine, and Art*, vol. 2, no. 1, p. 7, 2019.
- [23] R. C. Gonzalez, R. E. Woods, and S. L. Eddins, *Digital image processing using MATLAB*. Pearson Education India, 2004.
- [24] A. K. Jain, *Fundamentals of digital image processing*. Prentice-Hall, Inc., 1989.
- [25] J. Benesty, J. Chen, and Y. Huang, "Study of the widely linear wiener filter for noise reduction," in *2010 IEEE International Conference on Acoustics, Speech and Signal Processing*. IEEE, 2010, pp. 205–208.
- [26] I. Pitas and A. N. Venetsanopoulos, *Nonlinear digital filters: principles and applications*. Springer Science & Business Media, 2013, vol. 84.
- [27] S. Paris, P. Kornprobst, J. Tumblin, and F. Durand, *Bilateral filtering: Theory and applications*. Now Publishers Inc, 2009.
- [28] L. I. Rudin, S. Osher, and E. Fatemi, "Nonlinear total variation based noise removal algorithms," *Physica D: nonlinear phenomena*, vol. 60, no. 1-4, pp. 259–268, 1992.
- [29] G. Gilboa and S. Osher, "Nonlocal operators with applications to image processing," *Multiscale Modeling & Simulation*, vol. 7, no. 3, pp. 1005–1028, 2009.
- [30] I. Markovsky and K. Usevich, *Low rank approximation*. Springer, 2012, vol. 139.
- [31] O. Ronneberger, P. Fischer, and T. Brox, "U-net: Convolutional networks for biomedical image segmentation," in *International Conference on Medical image computing and computer-assisted intervention*. Springer, 2015, pp. 234–241.
- [32] C.-Y. Liou, W.-C. Cheng, J.-W. Liou, and D.-R. Liou, "Autoencoder for words," vol. 139. Elsevier, 2014, pp. 84–96.
- [33] G. E. Hinton, A. Krizhevsky, and S. D. Wang, "Transforming autoencoders," in *International conference on artificial neural networks*. Springer, 2011, pp. 44–51.
- [34] P. Vincent, H. Larochelle, I. Lajoie, Y. Bengio, P.-A. Manzagol, and L. Bottou, "Stacked denoising autoencoders: Learning useful representations in a deep network with a local denoising criterion," *Journal of machine learning research*, vol. 11, no. 12, 2010.
- [35] I. Laina, C. Rupprecht, V. Belagiannis, F. Tombari, and N. Navab, "Deeper depth prediction with fully convolutional residual networks," in *2016 Fourth international conference on 3D vision (3DV)*. IEEE, 2016, pp. 239–248.
- [36] Y. Xu, B. Du, L. Zhang, D. Cerra, M. Pato, E. Carmona, S. Prasad, N. Yokoya, R. Hänsch, and B. Le Saux, "Advanced multi-sensor optical remote sensing for urban land use and land cover classification: Outcome of the 2018 ieec grss data fusion contest," *IEEE Journal of Selected*

Topics in Applied Earth Observations and Remote Sensing, vol. 12, no. 6, pp. 1709–1724, 2019.

- [37] M. Cramer, “The dgpf-test on digital airborne camera evaluation—overview and test design,” *Photogrammetrie-Fernerkundung-Geoinformation*, vol. 2010, no. 2, pp. 73–82, 2010.
- [38] M. Gerke, “Use of the stair vision library within the isprs 2d semantic labeling benchmark,” 2014.
- [39] I. Sobel, “An isotropic 3x3 image gradient operator,” *Presentation at Stanford A.I. Project 1968*, 02 2014.
- [40] M. Abadi, A. Agarwal, P. Barham, E. Brevdo, Z. Chen, C. Citro, G. S. Corrado, A. Davis, J. Dean, M. Devin *et al.*, “Tensorflow: Large-scale machine learning on heterogeneous distributed systems,” *arXiv preprint arXiv:1603.04467*, 2016.
- [41] D. P. Kingma and J. Ba, “Adam: A method for stochastic optimization,” *arXiv preprint arXiv:1412.6980*, 2014.
- [42] D. Cerra, M. Pato, E. Carmona, S. M. Azimi, J. Tian, R. Bahmanyar, F. Kurz, E. Vig, K. Bittner, C. Henry *et al.*, “Combining deep and shallow neural networks with ad hoc detectors for the classification of complex multi-modal urban scenes,” in *IGARSS 2018-2018 IEEE International Geoscience and Remote Sensing Symposium*. IEEE, 2018, pp. 3856–3859.
- [43] Y. Xu, B. Du, and L. Zhang, “Multi-source remote sensing data classification via fully convolutional networks and post-classification processing,” in *IGARSS 2018-2018 IEEE International Geoscience and Remote Sensing Symposium*. IEEE, 2018, pp. 3852–3855.
- [44] K. He, X. Zhang, S. Ren, and J. Sun, “Deep residual learning for image recognition,” in *Proceedings of the IEEE conference on computer vision and pattern recognition*, 2016, pp. 770–778.
- [45] K. Simonyan and A. Zisserman, “Very deep convolutional networks for large-scale image recognition,” *arXiv preprint arXiv:1409.1556*, 2014.
- [46] G. Huang, Z. Liu, L. Van Der Maaten, and K. Q. Weinberger, “Densely connected convolutional networks,” in *Proceedings of the IEEE conference on computer vision and pattern recognition*, 2017, pp. 4700–4708.
- [47] A. Kendall, V. Badrinarayanan, and R. Cipolla, “Bayesian segnet: Model uncertainty in deep convolutional encoder-decoder architectures for scene understanding,” *arXiv preprint arXiv:1511.02680*, 2015.



Xinming Huang received his Ph.D. degree in electrical engineering from Virginia Tech, in 2001. He was a Member of Technical Staffs with the Wireless Advanced Technology Laboratory, Bell Labs of Lucent Technologies. Since 2006, he has been a Faculty Member with the Department of Electrical and Computer Engineering, Worcester Polytechnic Institute (WPI), where he is currently a Full Professor. His main research interests include the areas of circuits and systems, with an emphasis on reconfigurable computing, wireless communications, information security, computer vision, and machine learning.



Mahdi Elhousni is currently pursuing a PhD in Electrical and Computer Engineering at the Worcester Polytechnic Institute in Worcester, MA, USA. Before joining WPI, he had received a BS in computer science and a MS in embedded systems from the National school For Computer Science in Rabat, Morocco. His main research interest are computer vision, deep learning and SLAM.



Ziming Zhang is an assistant professor at Worcester Polytechnic Institute. Before joining WPI he was a research scientist at Mitsubishi Electric Research Laboratories (MERL) in 2016-2019. Prior to that, he was a research assistant professor at Boston University. Dr. Zhang received his PhD in 2013 from Oxford Brookes

University, UK, under the supervision of Prof. Philip H. S. Torr (now in the University of Oxford). His research areas lie in computer vision and machine learning, especially in object recognition/detection, data-efficient learning (e.g. zero-shot learning) and applications (e.g. person re-identification), deep learning, optimization. His works have appeared in PAMI, CVPR, ICCV, ECCV, NIPS. He serves as a review/PC member for top conferences (e.g. CVPR, ICCV, NIPS, ICML, ICLR, AAAI, AISTATS, IJCAI) and journals (e.g. PAMI, IJCV, JMLR). He won the R&D100 Award 2018.